Automation, Control and Intelligent Systems
2013; 1(6): 121-130
Published online January 30, 2014 (http://www.sciencepublishinggroup.com/j/acis)
doi: 10.11648/j.acis.20130106.11

Multiplexed spatiotemporal communication model in artificial neural networks

Shinichi Tamura[1, 2, *], Yoshi Nishitani[2], Takuya Kamimura[3], Yasushi Yagi[3], Chie Hosokawa[4], Tomomitsu Miyoshi[2], Hajime Sawai[2], Yuko Mizuno-Matsumoto[5], Yen-Wei Chen[6]

[1]NBL Technovator Co., Ltd, 631 Shindachimakino, Sennan City, 590-0522 Japan
[2]Graduate School of Medicine, Osaka University, Suita, 565-0871 Japan
[3]ISIR, Osaka University, 8-1 Mihogaoka, Ibaraki City, Osaka, 567-0047 Japan
[4]AIST Kansai, 1-8-31 Midorigaoka, Ikeda 563-8577 Japan
[5]Graduate School of Applied Informatics, University of Hyogo, Kobe, 650-0047 Japan
[6]Graduate School of Sci. and Eng., Ritsumeikan University, Kusatsu, 525-8577 Japan

Email address:
tamuras@ nblmt.jp(S. Tamura)

To cite this article:
Shinichi Tamura, Yoshi Nishitani, Takuya Kamimura, Yasushi Yagi, Chie Hosokawa, Tomomitsu Miyoshi, Hajime Sawai, Yuko Mizuno-Matsumoto, Yen-Wei Chen. Multiplexed Spatiotemporal Communication Model in Artificial Neural Networks. *Automation, Control and Intelligent Systems.* Vol. 1, No. 6, 2013, pp. 121-130. doi: 10.11648/j.acis.20130106.11

Abstract: It is well known that there is intercommunication among the different areas of the brain. However, till date, the rules of communication have not been successfully analyzed. The spike trains from neuronal cells have been simply treated as density-modulated waves with an activation level of the corresponding neuronal cells, or, at most, they have been analyzed using traditional metrics between sequences. The spike trains from neuronal cells have a random-like pattern that provides few clues regarding a coding rule. Here in a randomly generated artificial 3 × 3 multiplexed spatiotemporal communication neural network composed of threshold elements, we showed that pseudorandom sequences were generated during the simulation, similar to the random sequences generated by the cultured neural network of the rat brain. The transiently generated sequence patterns in the simulation were regarded as reflecting the circuit structure. These randomly shaped circuits generated pseudorandom sequences that functioned as codes for multiplexing communication. Although the circuit weights are randomly generated at present, it will be possible to extend this approach to determine the network weights by learning. This paper provides simulation results that support findings on cultured neural network.

Keywords: M-Sequence, Neural Network, Pseudo Random Sequence, Spatiotemporal Communication, Spike Train

1. Introduction

We have developed a time-shift diagram method [1] for visualizing the propagation of brain waves. Figure 1 shows an example of a time-shift diagram in which the transmissions of magnetoencephalography (MEG) waves for a number counting task are shown with propagation times of less than 5 [ms] (in red; mainly within each hemisphere) and more than 10 [ms] (in blue; mainly across the callosum) [2]. Propagation times of 5–10 [ms] are indicated in green. When compared with the MRI dipole diagram method, which shows only a small number of major flows, our method follows an even smaller flow of signals. Questions arise as to how neuronal cells find their target cells and how the target cells obtain the necessary signals from the source neurons even if they are located at remote positions. Such multi-access communication requires codes. This issue served as the motivation for our research. However, till date, the rules of communication in the brain have not been successfully analyzed. The spike trains from neuronal cells have been treated simply as density-modulated waves with an activation level of the corresponding neuronal cells, and, at best, they have been analyzed using traditional metrics between sequences and from the viewpoint of spatial independent information.

1.1. Research on Spike Coding

To analyze spike trains, metrics between spike trains have been proposed via an alignment of distances and convolution metrics, including traditional rate coding [3]. However, the coding scheme of neurons has not been solved.

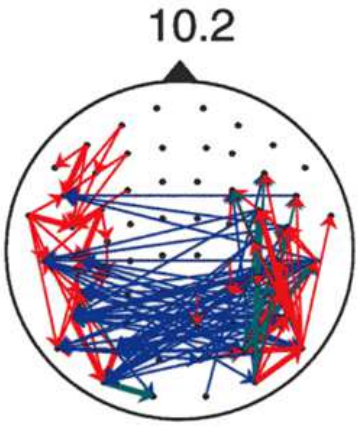

Figure.1. *Time-shift diagram of 10.2 Hz MEG for a number-counting task; lag time < 5 ms (red) was primarily within each hemisphere and lag time > 10 ms (blue) was across the callosum. Green: between 5–10 ms.*

1.2. Spatiotemporal Coding

The extension of signals in a multidimensional manner permits dealing with many spatiotemporal patterns in artificial and natural neural networks [4-7]. In the visual system in particular, directional receptive fields, as seen in mammalian simple cells, emerge by a minimum information criterion [8] and an independent component analysis [9] for natural and facial images, i.e., spatially independent basis functions are derived by self-organization. Figure 2 shows how the receptive fields of the visual system are obtained by self-organization of the neural circuit with mutual inhibition to output only independent components [10]. Thus, it is reasonable to seek the temporally independent components of information representation in the brain as a pair of spatially independent components or seek the spatiotemporal information representation and communication coding scheme.

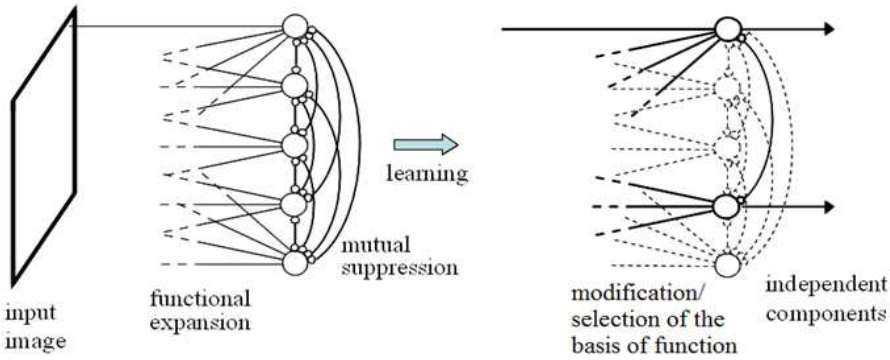

Figure.2. *Independent component extraction by mutual suppression in the visual system (dotted lines represent those that disappear after learning)*

1.3. Pseudorandom Codes from Cultured Neural Networks

We have been analyzing the spike train structure of cultured neural networks to clarify intelligent processing in the brain [11-13]. We have decoded the spike trains of several samples of neural networks cultured on 8 × 8 multi-electrodes. From these, we observed significantly more M-sequences than observed from interval shuffled trains, which are representative pseudorandom sequences.

The question as to why neuronal spike sequences have a white-noise like pattern, such as M-sequences, then arises. Although many researchers have been tackling this problem, it has not yet been solved. The objective of this study is to support these *in vivo* data via simulation.

The remainder of this paper is organized as follows: After presenting some background information in Section 2 (as well as in the Appendix), we propose a 3 × 3 spatiotemporal communication neural network model in Section 3 and present a discussion and conclusions in Section 4.

2. M-Sequence

An M-sequence is an important basis of communication theory and systems [14-17]. The electrical 3-cell linear feedback shift register (LFSR) shown in Fig. 3 cyclically generates the M-sequence “0010111” of length 7. The operation in the figure is performed by exclusive OR (xOR) according to the standard theory. Although there are some exceptional xOR neurons [18], this may be equivalently realized by the combination of threshold elements as a standard neuronal model. One such example is shown in the Appendix.

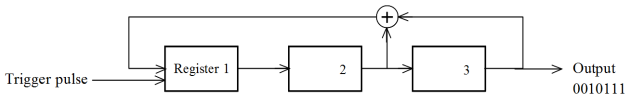

Figure 3. *Electrical linear feedback shift register with three logical elements (registers; cells) with an M-sequence output of length 7 (⊕ shows an Exclusive OR operation)*

The length of the M-sequence generated from n-cell LFSR is $2^n - 1$. In the case of a 3-cell LFSR, only one type of M-sequence exists, with the exception of mirror order and rotationally shifted sequences. We refer to this as M3, which is shown in Table 1. Table 1 also shows a 4-cell case (M4).

Table 1. *M3 and M4 M-sequences*

No. of Cells *n*	Regular /Reversal	Number and Comment	M-Sequence
3	Reversal (Rev)	(1)	1101000
		(2) mirror of (1)	1011000
	Regular (Non-Rev)	(3)	0010111
		(4) mirror of (3)	0100111
4	Reversal (Rev)	(5)	111011001010000
		(6) mirror of (5)	101001101110000
	Regular (Non-Rev)	(7)	000100110101111
		(8) mirror of (7)	010110010001111

Loop-shaped circuits, such as a LFSR, may become components of a large network or provide insights into larger loops in the intelligent network [19-22]. Furthermore, M-sequences are often used as codes in real communication systems, such as CDMA mobile phones, and may also become temporally independent components of information representation in the brain [10]. Therefore, we pay special attention to M-sequences as typical markers in the following sections and present some simulation results in the Appendix.

3. Communication Model in a Neural Network

3.1. Simplest Model

We can simulate brain neural networks as threshold-element (cell) networks. Figure 4 shows the simplest model of 2 × 2 spatiotemporal multiplexed communication. Each neuronal cell denoted by ○ works as one of these threshold elements in a synchronous mode, such that if the sum of the weighted inputs to the element is more than 0, it outputs "1," otherwise it outputs "0." Therefore, input "1" to n_1 is transmitted only to the opposite destination cell n_3, and input "1" to n_2 is transmitted to n_4.

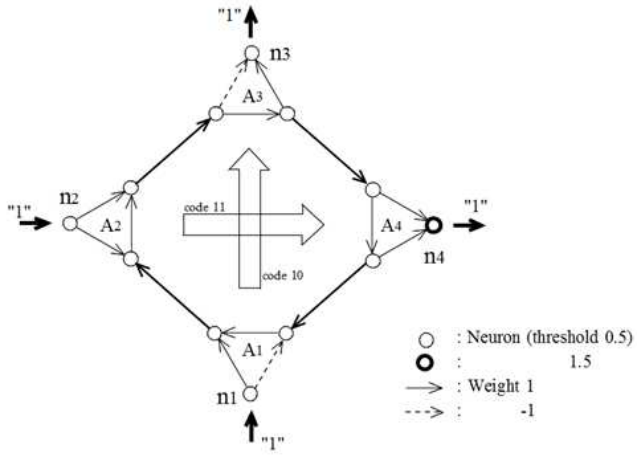

Figure 4. *Simple 2 × 2 spatiotemporal multiplex communication model*

3.2. 3 × 3 Spatiotemporal Multiplex Communication

As shown above, we can simulate brain neural networks using threshold element networks. In Fig. 5, we show a simple 3 × 3 communication model. With regard to the general behavior of synchronous threshold element networks, please refer to the Appendix.

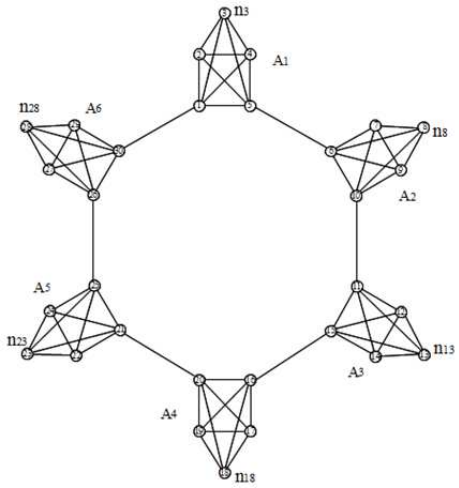

Figure 5. *A 3 × 3 communication model. Pulse "1" sent from neuron n_3 is supposed to be received only by n_{18}, that sent from n_8 is supposed to be received by n_{23}, and that sent by n_{13} is supposed to be received by n_{28}.*

Here, signal "1" sent from cell n_3 is not supposed to be received by n_8, n_{13}, n_{23}, and n_{28}. Signal "1" is to be received only by n_{18}. Similarly, the n_8 signal is supposed to be received by n_{23}, while that of n_{13} is supposed to be received by n_{28}. Each neuronal assembly of A_1, A_2, ..., A_6 is set to be able to work to encode or decode the signal. Main loops $\{n_1\text{-}n_5\text{-}n_6\text{-}n_{10}\text{-}n_{11}\text{-}n_{15}\text{-}n_{16}\text{-}n_{20}\text{-}n_{21}\text{-}n_{25}\text{-}n_{26}\text{-}n_{30}\text{-}n_1\}$ are set to give not one but two paths to any communication channels of $n_3 \rightarrow n_{18}$, $n_8 \rightarrow n_{23}$, and $n_{13} \rightarrow n_{28}$, i.e., each assembly works to encode/decode the signal and to pass such signals through that are not for its output neuron. Then, the signal can be spatiotemporally encoded.

3.2.1. Wide Time Gate

We generated networks with random weights ($\in \{+1, 0, -1\}$) and selected those that satisfied the requirements mentioned above. We generated 2.012×10^8 networks in which each weight on the main loop was bidirectionally fixed to +1, i.e., weights from n_5 to n_6 and n_6 to n_5 were +1, and so on. Other weights were randomly fixed to +1, 0, and −1, with probabilities of 1/3 for each.

All cells in the network were synchronously driven. A single pulse "1" was given to the n_3 cell at time 1, and the output number of "1" was counted between time 1 and 16 at the n_{18} cell. Effectively, the count was between times 8 and 16 at the destination cell because the pulse arrived at time 8. If the number of output "1" is the largest among $\{n_8, n_{13}, n_{18}, n_{23}, n_{28}\}$, successful communication is achieved for the test of the $n_3 \rightarrow n_{18}$ channel. If the three communication channels of $n_3 \rightarrow n_{18}$, $n_8 \rightarrow n_{23}$, and $n_{13} \rightarrow n_{28}$ are all successful in the same network, we classified the network as being

successful in the 3 × 3 multiplex communication.

We obtained 141 successful networks with the desired function, i.e., the success rate was 7.01×10^{-7} or, in other words, one network per 1.43×10^{6} randomly generated networks exhibited 3 × 3 spatiotemporal multiplex communication.

Figure 6 shows an example of a successful network. Figure 7 shows the flow of the codes that worked as markers of the information flow; almost all sequences generated from a cell were transient within the short time of the communication and were too long to analyze. Thus, to visualize the information flow, we selected several remarkable short codes with length $\leqq 7$ from the observed propagating wavefront sequence. We marked sequences "1011," "10101," "11111," and "0010111." "1011" is a core part of the reversal M-sequence "1011000;" "10101" is a typical alternating sequence of "0" and "1;" "11111" is a representative of long continuous "1" sequences; and "0010111" is a conventional non-reversal M-sequence.

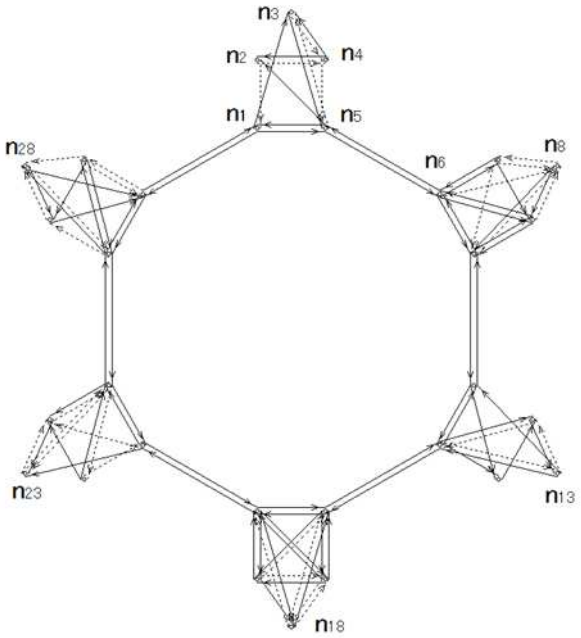

Figure 6.. *Example of a network realizing 3 × 3 spatiotemporal multiplex communication (solid lines indicate a weight of +1 and dotted lines indicate a weight of −1)*

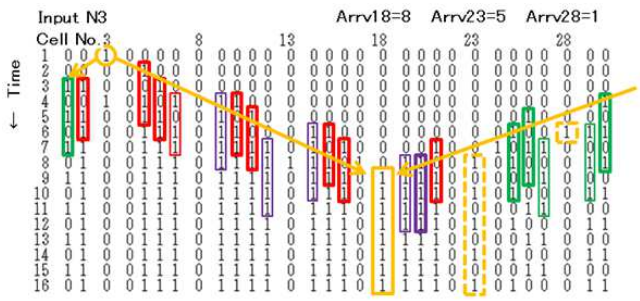

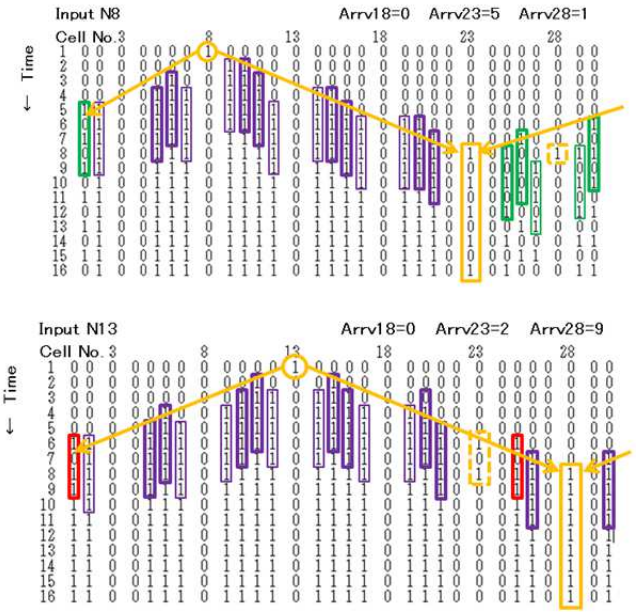

Figure 7. *State transition diagram of the multiplex communication network shown in Fig. 6 with a wide time gate, where "1" is the input to n_3 (top), n_8 (middle), and n_{13} (bottom). It can be considered that the source input "1" is encoded to "1011," "11111," and "10101" and finally gives the maximum output at the destination n_{18} (top), n_{23} (middle), and n_{28} (bottom), respectively.*

Input stimulation to one of $\{n_3, n_8, n_{13}\}$ was encoded by the corresponding cell assembly $\{A_1, A_2, A_3\}$ and spreads in both directions to the right and left of the loop. Sometimes they were transformed to another code at the passing cell assembly, decoded at the destination assembly, and transmitted to the destination cell. If the coming sequence is not for its assembly, the assembly does not take it in but passes it to the next assembly.

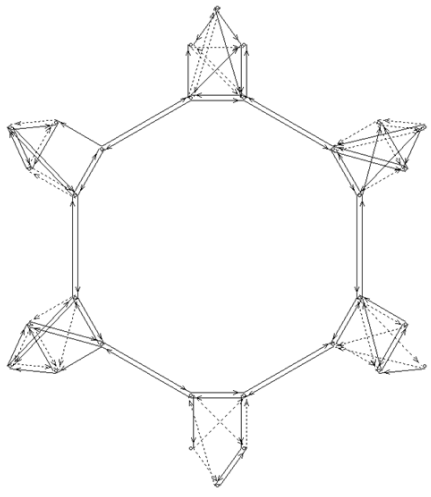

Figure 8. *Another example of network weight realizing a 3 × 3 communication*

Figures 8 and 9 show another example. Here, a conventional non-reversal M-sequence, "0010111," and reversal M-sequences, "1010001" and "0100011," were generated by the initial source input pulse "1" to the n_{13} cell.

However, only the first code contributed to the output via an anticlockwise rotation route, whereas latter codes via a clockwise rotation route did not contribute. The maximum output was given from the destination cell n_{28}.

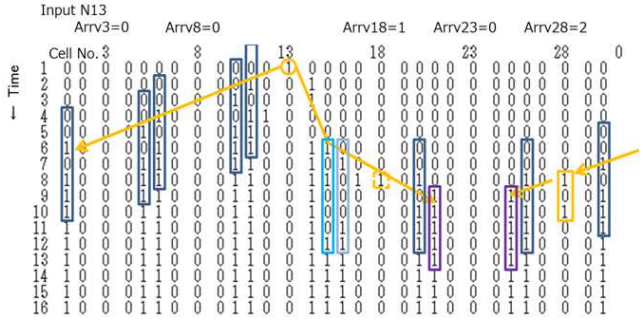

Figure 9. *State-transition diagram of the communication network shown in Fig. 8. "1" is given to n_{13}, which is internally encoded to the M-sequences "0010111," "1010001," and "0100011."*

The temporal response function (time gate) at the receiving cell is shown in Fig. 10. In the case of a wide time gate, the number of "1s" at the destination cell is effectively counted after time 8, which represents the fastest arrival time of the pulse.

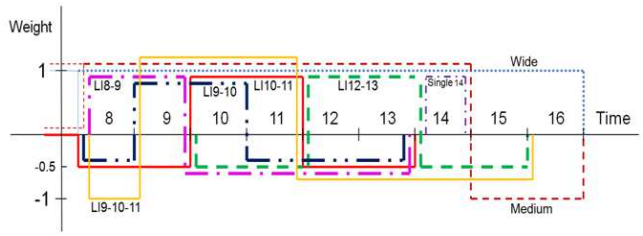

Figure 10. *Time gate weights at a receiving cell. Time 8 is the fastest arrival time of the pulse at the destination cell. In the case of a single time gate, only time 14 is shown. Double and triple time gates, which are the central part of LI-type gates, are not shown.*

3.2.2. Medium Time Gate

In the network described in Section ***3.2.1***, the gate only counted the number of pulses that arrived at the destination cell during the observation period from time 1 to 16. In the medium time gate, we restricted the arrival period at the receiving cell, i.e., the "1s" that arrived at times 15 and 16 were counted as penalties, and their number was subtracted from the number of "1s" that arrived between times 1 and 14 (roughly counting pulses between time 8 and 12; see Fig. 10 Medium). We obtained 222 successful networks from the 2.295×10^8 generated candidate networks. The success rate was 9.67×10^{-7}, or, in other words, one network per 1.03×10^6 generated candidate networks met the required communication function. This figure was higher than that of the wide time gate. However, we consider that such communication tasks are still difficult. Figure 11 shows the number of codes of "1011," "11111," "10101," and "1101" obtained at the pulse wavefront on the main loop. This result shows that rate distribution was influenced by the task of the network. There was a definite difference between the appearance average rates of "1011" of the wide time gate network and those of the medium time gate as an ensemble. However, because the appearance rates had large standard deviations, the average difference was not particularly important. In other words, there are many ways to realize a given task, as shown by the large standard deviations depicted in Fig.12, and the appearance rate reflects the structural difference only as an average.

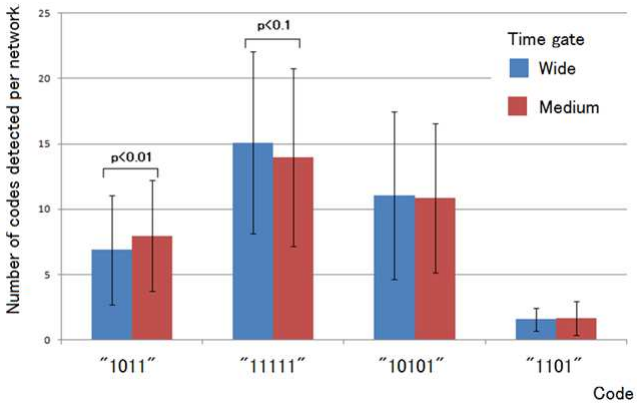

Figure 11. *Major code spectrum of wide and medium time gate communication networks*

3.2.3. Single Time Gate

In this case, we imposed a restriction of the time gate to specific single times of 8, 9, 10, 13, and 15. The corresponding success rates are shown in Fig. 12.

Figure 12. *Success rate of a random network for the communication tasks*

3.2.4. Double and Triple Time Gates

In case of a double time gate, we combined two single time gates, such as D8–9, D9–10, D10–11, and D12–13. The corresponding success rates are shown in Fig. 13; the success rates of the double time gate are close to the average of the corresponding single time gates. Furthermore, we combined three single time gates, such as T9–10–11. In this case, the success rate was higher than that of each of the corresponding single time gates.

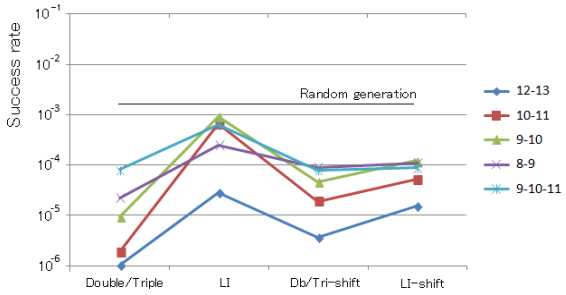

Figure 13. *Success rates of a randomly generated network for a 3 × 3 communication task with double/triple, LI gates, and their time shift gates. "Random generation" is a theoretical upper limit of a randomly generated network that can attain the given task by chance.*

3.2.5. Lateral Inhibition (LI) Type Time Gate

Because the LI-type response is universal in natural neural networks, we applied it to the time response of the receiving cells.

The central peak was fixed to weight 1 and width 2. The central positions were taken at times 8–9, 9–10, 10–11, and 12–13. Four negative bases on both sides were set at a weight of −0.5. However, because the pulse arrived first at the destination cell at time 8, the front negative bases before time 8 were moved to the tail, as shown in Fig. 10. Each weight from time 8 to 16 was:

LI8–9 = (1, 1, −0.5, −0.5, −0.5, −0.5, 0, 0, 0)
LI9–10 = (−0.5, 1, 1, −0.5, −0.5, −0.5, 0, 0, 0)
LI10–11 = (−0.5, −0.5, 1, 1, −0.5, −0.5, 0, 0, 0)
LI12–13 = (0, 0, −0.5, −0.5, 1, 1, −0.5, −0.5, 0).

The code spectrum obtained is shown in Fig. 14. Some average differences existed between these LIs. However, the standard deviations were close to these averages; therefore, we could only observe almost random pulse sequences. The situation was the same in the cases of a single time gate described in *3.2.3* in which the spectra were almost the same as those shown in Fig. 14.

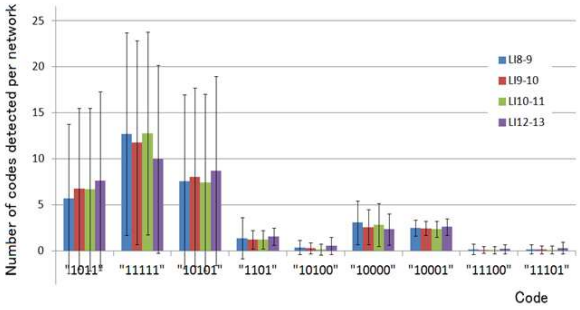

Figure 14. *Code spectrum with standard deviation on the main loop of LI-type time gate communication networks*

The weight of the LI-type triple time gate was set as LI9–10–11 = (−1, 1, 1, 1, −0.5, −0.5, −0.5, −0.5, 0).

3.2.6. Time Shift Gate

The time-gate settings described above may create a bias to give the destination cell the maximum output, while potentially giving the non-destination cell located nearest to the source cell a lower output for pulses arriving through the shorter main loop route. To compensate for this bias, we shifted the center of the time gate of the halfway cells by 2, 4, and 6 according to the distance from the source cell. However, this remains incomplete at the point at which the pulses arriving through the longer main loop route are neglected.

3.3. Success Rate for Communication

We randomly generated networks, and if the network randomly gave the communication pair, the success rate ideally should become $5^{-3} = 1.6 \times 10^{-3}$. However, the success rate of these networks with regard to communication was significantly different according to the type of time gate, as is shown in Figs. 12 and 13. The success rate of the wide time gate was the worst. In this time gate, there was no restriction on the arrival time of pulses, and only the pulses arriving at the receiving cell were counted. Single time gates, double time gates, and triple time gates had a better success rate. Among these, the faster time gate was relatively good. The LI-type time gates had the best success rate. In cases of LI9–10, LI10–11, and LI9–10–11, the success rate was approximately 10^{-3}. The improvement in detectability according to the time-gate shape had two effects on the success rate. One is the direct effect of raising the success rate. The other is lowering the success rate by raising the detectability of non-destination cells.

Figure 13 shows the success rates of time shift gates for double-type, triple-type, and LI-type time gates. LI-type time gates seemed to be sufficiently powerful for detecting the proper sequence. The time shift gates raised the detectability of non-destination cells, thus reducing the success rates. This shows that a bias of the time gate adjusted for destination cells helped detection at the destination cell. Figure 15 shows an example of a state-transition diagram of an LI-type time shift gate case.

The success rates of all time gates were lower than 5^{-3} of the ideal random channel selection. The reasons for this observation may be that the random lines are sometimes disconnected, the network outputs the same levels, and the three directional tasks are not independent. However, LI-type reception is commonly effective in spatiotemporal communication with high success rates close to the ideal rate as well as in other general neural networks.

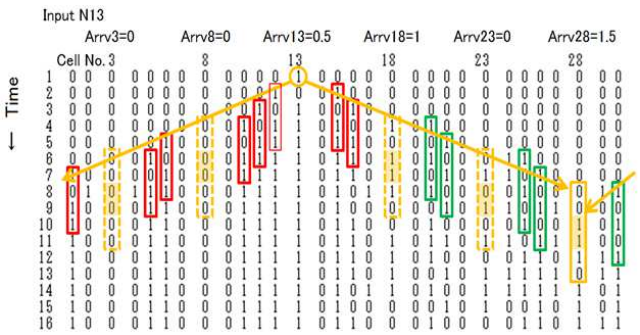

Figure 15. *Example of a state-transition diagram for a stimulation where "1" is given to n_{13} and an LI-type time shift gate is used*

4. Discussion and Conclusions

We believe that the communication function between neuronal cells provides a basis for the intelligence functions of the brain, such as memory, association, and abstraction. However, to date, the neuronal spike trains have been treated as random noise-like signals, and the coding scheme of the natural neural network has not been completely elucidated. We have been tackling this issue from a communication engineering viewpoint and have proposed a model of spatiotemporal multiplex communication. In this model, each cell works as a transmitting/receiving cell and as a relay cell, the roles of which are I/O and intermediate communication, respectively. In this sense, the network works like a multi-hop ad hoc communication network.

Although only the shape of the network is given by 3 × 3 spatiotemporal multiple communication loop types, various network shapes can be considered; for example, a homogeneous network without a pre-assigned loop. Moreover, there are various ways to determine the task of the communication, i.e., various possible network shapes can have additional routes to the destination and timings. This represents a problem of balance between space and time.

We have shown that the simulated pulse sequence from each cell of the threshold element network resembled our experimental data, including the code spectrum. However, though not shown here, our experimental data were obtained in an unsorted state, including a single neuronal cell, and several neuronal cells and cell assemblies, such as synfire chains [23,24], which may cause synchronous spikes, including codes. Codes may be composed from these cell "groups," which represents an open problem.

We obtained target networks via random generation and selection. Although this method is useful to demonstrate the feasibility of such communication tasks, it is ineffective in real situations because of necessary computational capacity. In the brain, target networks are considered to be formed by learning. Therefore, we are now developing such networks based on learning. In addition, noise immunity, interference effects between communication channels and successive transmissions, and stability should be investigated. However, the objective of this paper is to demonstrate the feasibility of spatiotemporal multiplex communication in neural networks, and we believe we were able to show its feasibility using a minimum-size model.

The content of this paper can be summarized as follows:

1) A neural network with a spatiotemporal communication function was proposed.

2) Each neuronal cell worked as a transmitting and receiving cell as well as a relay cell.

3) Pulses running in the network seemed to be like noise, similar to the code observed in naturally cultured neuronal networks.

Appendix

Here, we present some results of an output analysis, particularly for the M-sequences included in the state transition output of each threshold element of the network in general.

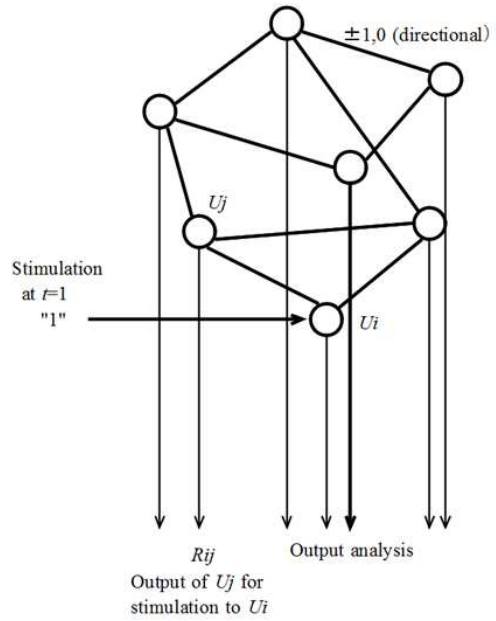

Figure A1. *Output analysis of threshold cell network*

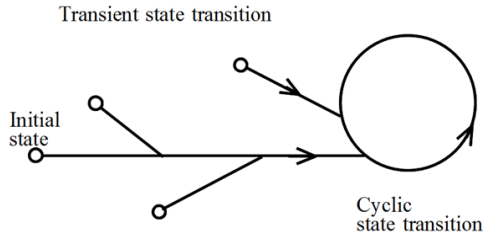

Figure A2. *State transition of the network*

Figure A1 shows the method used to analyze the output of the network. At time t = 1, a single stimulation "1" is given to cell U_i; $i \in \{1, 2, \ldots, n\}$, where n is the number of cells. Cell U_j; $j \in \{1, 2, \ldots, n\}$ gives an output of "0" if the sum of the weighted input given to U_j is $\leqq 0$ and "1" if this sum is > 0 synchronously in the network. The threshold is 0 unless otherwise specified. Each weight is +1, 0, or −1. Generally, the state expressed by the combination of all cell states ("0" or "1") changes with time, as shown in Fig. A2.

A1. Four-Cell Network

In this case, all possible $3^{16} = 43{,}046{,}721$ networks could be generated non-randomly as a treatable maximum number. Although we did not use this approach, this number may be reduced by using the symmetric characteristic of the weights. Instead, stimulation was given only to a fixed cell, e.g., U_1.

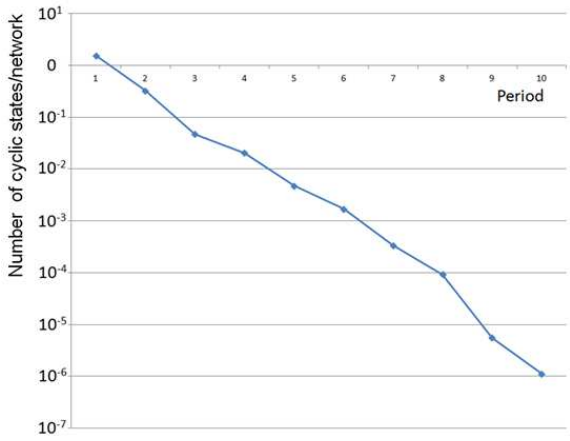

Figure A3. *Period distribution of cycles of state transition in a 4-threshold-cell network*

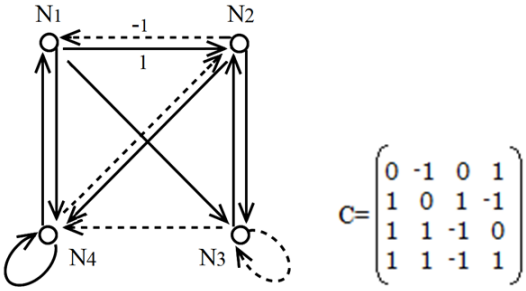

Figure A4. *Threshold cell network with weights of ±1 and 0, which generates the M-sequence "1001110" from N_1 for stimulation of "1" to N_1*

The average number of cycles of state transition per network is shown in Fig. A3. Period 1 means that the state did become stationary. Some networks generated an M-sequence (see Fig. A4 for an example). The i, j entry of matrix $\boldsymbol{C}$ shows the connection weight from N_j to N_i. The output sequence from N_1 is "1001110," which is an inverse-order, rotationally-shifted, and non-reversed version of the M-sequence "1101000" listed in Table 1.

A2. Number of M-Sequences Detected

The output from each cell was checked among 32 clock times after stimulation. Then, the total number of 1.34×10^{10} positions on the sequences was checked. The detected M-sequences are shown in Table A1, in which (1)–(4) correspond to those listed in Table 1. In this case, the rate of Non-Rev was larger than that of Rev.

A3. Twelve-Cell Network

In this case, we were no longer able to check all networks. Thus, we generated networks with various weights {+1, 0, −1}, as shown in Table A1. By changing the stimulation cell, the output from each cell was checked among 64 (practically 52 time positions) clock times after the stimulation.

Table A1. *Rate of M-sequences detected*

No. of Cells n	Possible Networks	Rate of Weights +1, 0, −1	Generated Networks	Sequence Positions Checked $\times 10^6$	Rate of M3 (length 7) Rev [(1), (2)] $\times 10^{-3}$	Rate of M3 (length 7) Non-Rev [(3), (4)] $\times 10^{-3}$
4	3^{16}	(All Checked) Equivalently 1/3, 1/3, 1/3	3^{16}	13,400	6.61 (4.47, 2.14) $\times 10^{-5}$	16.6 (5.00, 11.6) $\times 10^{-5}$
		0.4, 0.2, 0.4	6000	44.9	12.0 (6.08, 5.89)	9.95 (4.88, 5.07)
		0.3, 0.4, 0.3	6000	44.9	11.1 (5.59, 5.46)	8.44 (4.22, 4.22)
12	3^{144}	0.1, 0.8, 0.1	3000	22.4	1.53 (0.785, 0.749)	0.912 (0.456, 0.456)
		0.15, 0.8, 0.05	23,000	172	3.32 (1.56, 1.76)	2.94 (1.69, 1.25)
		0.06, 0.92, 0.02	9,000	67.4	0.117 (0.0472, 0.0702)	0.0802 (0.0561, 0.0241)

Figure A5 shows a time flow for the case of the weight rate of (0.1, 0.8, 0.1). Here, "Theor" represents the theoretical values calculated for cases in which the observed sequence was white random (no correlation within the sequence) and the observed "0" and "1" rates were used at each time position. The observed rates of the M-sequence code were rather low, with the exception of the initial time area. This means that the states at the initial time area are transient and close to the random state. In addition, after some time, the states shift to steady states that include final cyclic states, most of which are not M-sequence cycles, but are shorter (such as "1111111," "0000000," or "101010101").

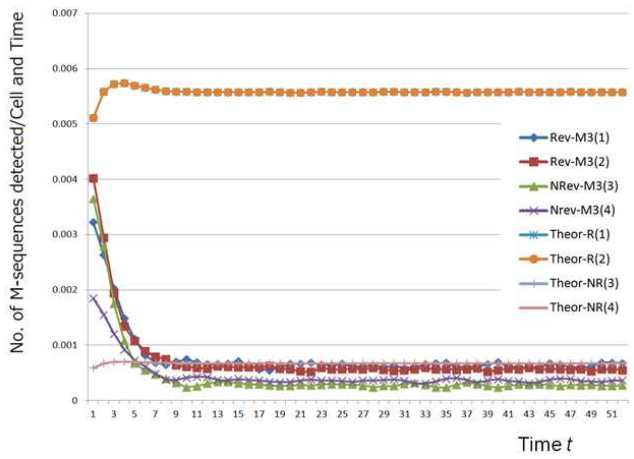

Figure A5. *Number of M-sequences detected per cell and time. Symbols correspond to those listed in Table 1. "Theor" refers to the theoretical values under the assumption of a random sequence. Curves of Theor-(1) and (2) almost overlap. Curves of Theor-(3) and (4) also almost overlap.*

As a result, we can say that there was a tendency for the rate of Rev M-sequences, including those that are fragmental, to be greater than that of Non-Rev sequences. In addition, information from the source cell was included in the early transient period. This explains why we analyzed only the wavefront in this study.

Acknowledgements

The authors are grateful to Dr. T. Shimosakon of Osaka Institute of Technology for his support and advice.

References

[1] Y. Mizuno-Matsumoto, K. Okazaki, A. Kato, T. Yoshimine, Y. Sato, S. Tamura, and T. Hayakawa., "Visualization of epileptogenic phenomena using cross-correlation analysis: Localization of epileptic foci and propagation of epileptiform discharges," IEEE Trans. Biomed. Eng. 46, pp.271-279, 1999.

[2] Y. Mizuno-Matsumoto, M. Ishijima, K. Shinosaki, T. Nishikawa, S. Ukai, Y. Ikejiri, Y. Nakagawa, R. Ishii, H. Tokunaga, S. Tamura, S. Date, T. Inouye, S. Shimojo, and M. Takeda, "Transient Global Amnesia (TGA) in an MEG Study," Brain Topography 13, pp.269-274, 2001.

[3] B. Cessac, H. Paugam-Moisy, T. Viéville, "Overview of facts and issues about neural coding by spikes," J. Physiol.-Paris 104, (1-2), pp.5-18, 2010.

[4] O. Kliper, D. Horn, B. Quenet, and G. Dror, "Analysis of spatiotemporal patterns in a model of olfaction," Neurocomputing 58-60, pp.1027-1032, 2004.

[5] K. Fujita, Y. Kashimori, and T. Kambara, "Spatiotemporal burst coding for extracting features of spatiotemporally varying stimuli," Biol. Cybern., 97, pp.293-305, 2007. DOI 10.1007/s00422-007-0175-z

[6] I. Tyukin, T. Tyukina, and C. van Leeuwen, "Invariant template matching in systems with spatiotemporal coding: A matter of instability," Neural Networks 22, pp.425-449, 2009.

[7] A. Mohemmed, S. Schliebs, S. Matsuda, and N. Kasabov, "Training spiking neural networks to associate spatio-temporal input–output spike patterns," Neurocomputing 107, pp.3-10, 2013.

[8] B.A. Olshausen and D.J. Field, "Emergence of simple-cell receptive field properties by learning a sparse code for natural images," Nature 381, pp.607-609, 1996.

[9] A. Bell and T. Sejnowski, "The independent components of natural scenes are edge filters," Vision Research 37, pp.3327-3338, 1997.

[10] S. Tamura, Y. Mizuno-Matsumoto, Y-W. Chen, and K. Nakamura, "Association and abstraction on neural circuit loop and coding," The Fifth International Conference on Intelligent Information Hiding and Multimedia Signal Processing (IIHMSP2009) A10-07(No.546) , Kyoto, September 12-14, 2009. Available: IEEE XPlore

[11] Y. Nishitani, C. Hosokawa, Y. Mizuno-Matsumoto, T. Miyoshi, H. Sawai, and S. Tamura "Detection of M-Sequences from Spike Sequence in Neuronal Networks," Computational Intelligence and Neuroscience 2012, Article ID 862579, 9 pages, 2012. doi:10.1155/2012/862579.

[12] S. Tamura, Y. Nishitani, C. Hosokawa, Y. Mizuno-Matsumoto, T. Kamimura, Y-W. Chen, T. Miyoshi, and H. Sawai, "M-sequence family from cultured neural circuits," The 3rd Int'l Workshop on Computational Intelligence for Bio-Medical Science and Engineering (CIMSE-2012), Taipei, October 23-25, 2012.

[13] S. Tamura, Y. Nishitani, C. Hosokawa, Y. Mizuno-Matsumoto, T. Kamimura, Y-W. Chen, T. Miyoshi, and H. Sawai, "Pseudo random sequences from neural circuits," IFMIA 2012, Daejeon, November 16-17, 2012.

[14] R.C. Dixon, Spread Spectrum Systems, John Wiley & Sons Inc., 1976.

[15] D.V. Sarwate and M. B. Pursley, "Crosscorrelation properties of pseudorandom and related sequences," Proc. IEEE 68, pp.593-619, 1980.

[16] S. Tamura, S. Nakano, and K. Okazaki, "Optical code-multiplex transmission by Gold-sequences," IEEE/OSA J. Lightwave Tech. 1, No.3, pp.121-127, 1985.

[17] S.W. Golomb and G. Gong, Signal Design for Good Correlation: For Wireless Communication, Cryptography, and Rader, Cambridge University Press, 2005.

[18] P. Fromherz and V. Gaede, "Exclusive-OR function of single arborized neuron," Biol Cybern 69, pp.337-344, 1993.

[19] C. Lecerf, "The double loop as a model of a learning neural system," Cybernetics and Informatics 1, pp.587-594, 1998.

[20] Y. Choe, "Analogical cascade: A theory on the role of the thalamo-cortical loop in brain function," Neurocomputing 52-54, pp.713-719, 2003.

[21] T. Kamimura, K. Nakamura, K. Yoneda, Y-W. Chen, Y. Mizuno-Matsumoto, T. Miyoshi, H. Sawai, and S. Tamura, "Information communication in brain based on memory loop neural circuit," ICIS2010 & SEDM2010, Chengdu, June 23-25, 2010. Available: IEEE Xplore

[22] T. Kamimura, Y-W. Chen, Y. Yagi, and S. Tamura, "Learning of Loop Neural Circuit for Memory," CIMSE2011, ICCIT2011, Jeju, November 29-December 1, 2011. Available: IEEE Xplore

[23] M. Abeles, Local Cortical Circuits: An Electrophysiological Study, Springer, Berlin, 1982.

[24] M. Abeles, "Synfire chains," Scholarpedia, 4(7), pp.1441, 2009.